Proceedings of the 12th International Symposium on Physics of Materials, Prague, September 4–8, 2011

AFM Observation of Fe–Al Single Crystals under *in situ* Deformation

J. Veselý[a,*], M. Cieslar[a] and J. Kopeček[b]

[a]Charles University in Prague, Faculty of Mathematics and Physics, Department of Physics of Materials
Ke Karlovu 5, 121 16 Praha 2, Czech Republic

[b]Institute of Physics AV ČR, v. v. i., Prague, Czech Republic

Fe–Al single crystals of three different compositions (20, 28 and 40 at.% Al) in single slip orientation were studied. Evolution of their surfaces during deformation at room temperature was observed *in situ* in atomic force microscope. Atomic force microscopy allows us to investigate slip lines on much finer scale than traditional optical observations. Wavy slip bands in Fe–Al_{20}, cross-slip in Fe–Al_{28} and weak slip line texture in Fe–Al_{40} are described. *Post mortem* observations of surfaces of Fe–Al_{28} deformed at elevated temperatures (in the range of yield stress anomaly) are presented as well.

PACS: 68.35.bd, 62.20.F−, 68.37.Ps

1. Introduction

Ordered intermetallic compounds in Fe-rich part of Fe–Al system (Fe_3Al and FeAl) show so called yield stress anomaly (YSA) [1]. They exhibit a temperature range where their yield stress increases with temperature. This makes them interesting for high temperature structural applications. They have been subject of extensive research, for a review see [2]. Still, the exact mechanism of YSA in these materials is not fully understood.

Atomic force microscopy (AFM) observation of dislocation traces on deformed surface could shed more light onto this problem as this method was already proved useful during the study of YSA in Ni_3Al [3].

Until now AFM has been utilized in several studies of Fe_3Al [4–6]. The information on its application to $B2$ FeAl [7] or *bcc* Fe alloys is scarce except for few studies of fatigue and cyclic deformations in steels [8]. Systematic AFM study of compounds in Fe-rich part of Fe–Al system with the focus on YSA is therefore missing.

In this article observations on the range of compositions and crystal structures (*bcc*, $B2$ and $D0_3$) are reported. In the case of Fe–Al_{28} observations obtained through the range of temperatures (including YSA regime) are reported as well.

2. Experimental procedure

Materials of nominal composition 20, 28, and 40 at.% Al balanced by Fe were prepared by arc melting of 99.995 wt% Al and 99.95 wt% Fe (main impurity being Mn). The Bridgman method was used to grow single crystals. After the growth, ingots were annealed at 1273 K for 4 h and furnace cooled.

Single crystal specimens of a nominal size $2\times2\times5$ mm^3 were cut from the ingots. Specimens were oriented by the Laue back-reflection X-ray diffraction with longest axis along [1 2 3] direction and faces parallel to $(2\,\bar{1}\,0)$ and $(3\,6\,\bar{5})$ planes. Fe–Al_{28} and Fe–Al_{40} specimens were further annealed for 140 h at 723 K and oil quenched. Fe–Al_{20} specimens were annealed for 24 h at 800 K.

Face parallel to the $(2\,\bar{1}\,0)$ plane was polished in several steps by diamond pastes (3, 1, and 1/4 μm) and finally by the suspension of colloidal silica (50 nm) to the roughness of about 1 nm (root mean square of 30×30 μm^2 area).

Specimens were deformed in compression along the longest axis in the apparatus described in [9]. Deformation was periodically stopped and contact mode AFM images of the same area were acquired. The interruptions lasted typically few minutes. The final plastic deformation was about 3%. Additional AFM images were acquired from different areas after the deformation test.

Furthermore, specimens of Fe–Al_{28} and Fe–Al_{40} were deformed at elevated temperatures (500, 700, 800, and 900 K) in an Instron machine and examined in the AFM after the test. These deformations were carried out under the flow of argon. The temperature had been equilibrated for at least 15 min before the tests. The strain rate was about 8×10^{-5} s^{-1} and matched the room temperature *in situ* experiments.

3. Experimental results

3.1. Fe–Al_{20}

We obtained images (Fig. 1) of slip bands in direction that roughly follows plane of maximum Schmid factor. However, slip bands are curved and thus their direction cannot be linked with any particular low index crystallographic plane. The formation of slip band from initially flat surface was captured on several images (Fig. 1a–d). After the final 3% of plastic strain (Fig. 1e–f) slip bands are about 5 to 10 μm wide with height in the order of hundreds of nanometers (the out of plane step created by single dislocation is about 0.2 nm). The areas between slip bands appear pristine.

* corresponding author; e-mail: vesely@gjh.sk

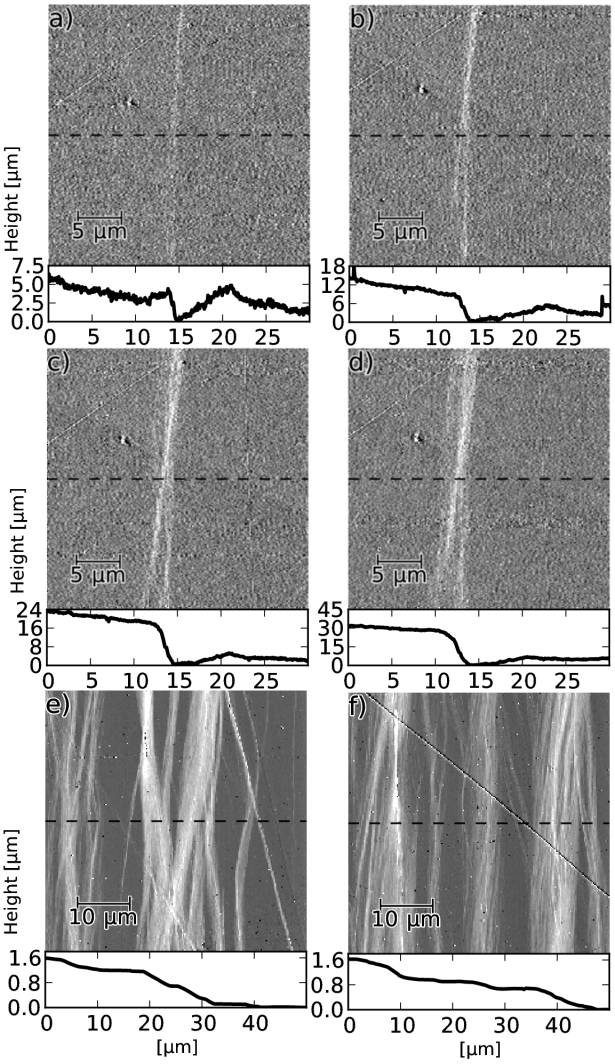

Fig. 1. Wavy slip bands in *bcc* Fe–Al_{20}: (a)–(d) formation of slip band at about 1% of global plastic strain; (e) and (f) developed structure after about 3% of plastic strain. Deformation axis is horizontal, AFM error signal, topography profile across the middle of the image (dashed line) is shown below the images.

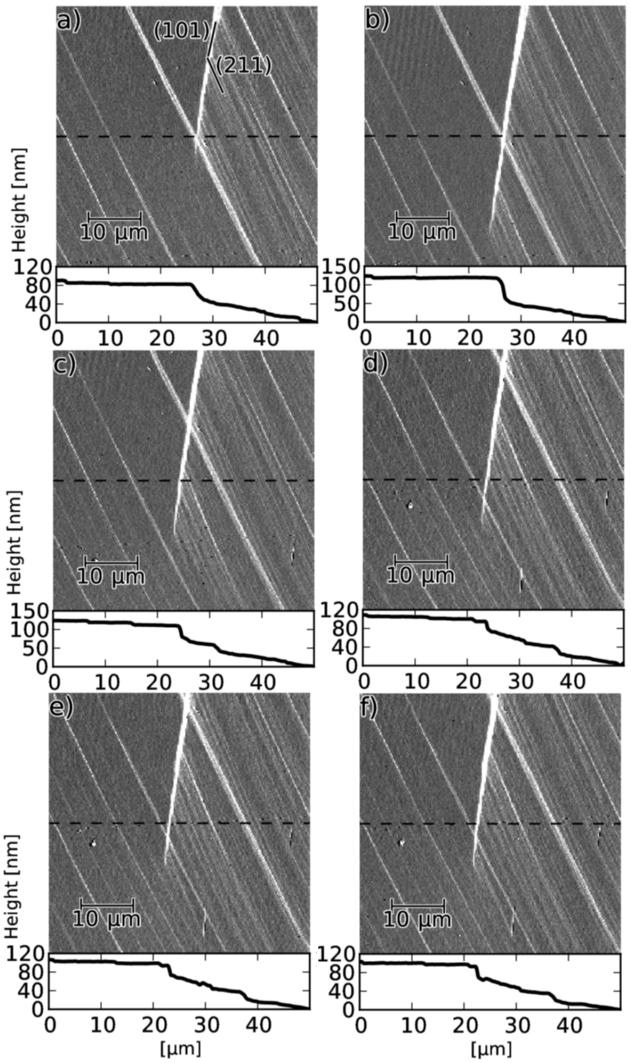

Fig. 2. Propagating tip of the primary slip band acts as the source of secondary slip lines in Fe–Al_{28}. Deformation axis is horizontal, AFM error signal, topography profile across the middle of the image (dashed line) is shown below the images.

3.2. Fe–Al_{28}

During the deformation of Fe–Al_{28} massive primary slip bands in the direction corresponding to the $[1\,\bar{1}\,\bar{1}](1\,0\,1)$ slip system were observed as well as finer lines corresponding to $[1\,\bar{1}\,\bar{1}](2\,1\,1)$ slip system. These secondary lines appeared to originate from primary slip bands (Fig. 2). *In situ* observation of the propagating tip of the slip band revealed that this is indeed the case: secondary slip lines were emitted from the tip of the propagating primary slip band.

Similarly to the Fe–Al_{20}, the deformation was localized within the slip bands and the areas between them remained in original polished state.

3.3. Fe–Al_{40}

In the early stage of deformation in this alloy, the surface was covered by very weak texture of slip lines corresponding to $[1\,\bar{1}\,\bar{1}](101)$ and $[1\,\bar{1}\,\bar{1}](1\,1\,0)$ slip systems (Fig. 3c). Both systems appeared almost equally active. As the deformation progressed the massive slip bands of first $[1\,\bar{1}\,\bar{1}](1\,0\,1)$ and then $[1\,\bar{1}\,\bar{1}](1\,1\,0)$ slip systems developed (Fig. 3a,b). The texture between the slip bands evolved only a little with the typical step height reaching no more than 2 nm after about 3% of strain.

3.4. Elevated temperature

Both Fe–Al_{28} and Fe–Al_{40} showed yield stress (stress at 0.2% plastic strain) anomaly with the peak at about 800 K, as can be seen in Fig. 4. In the case of Fe–Al_{40} the first drop of yield stress with temperature was only very weak.

The surface of Fe–Al_{40} deformed at high temperatures was severely oxidized. Therefore, only the results on

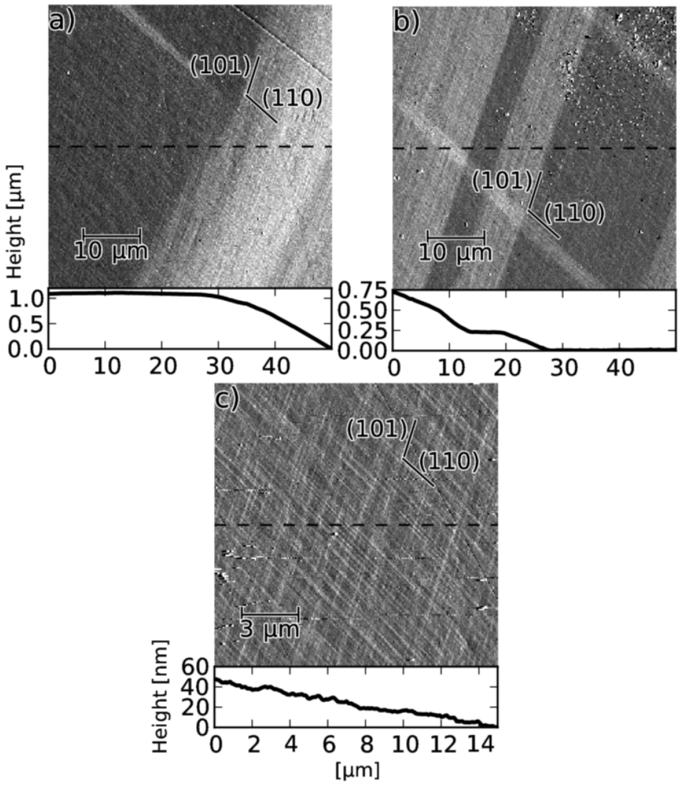

Fig. 3. Slip band structure in Fe–Al_{40}: (a) and (b) global view after about 3% of plastic strain; (c) detail of weak texture between the slip bands. Deformation axis is horizontal, AFM error signal, topography profile across the middle of the image (dashed line) is shown below the images.

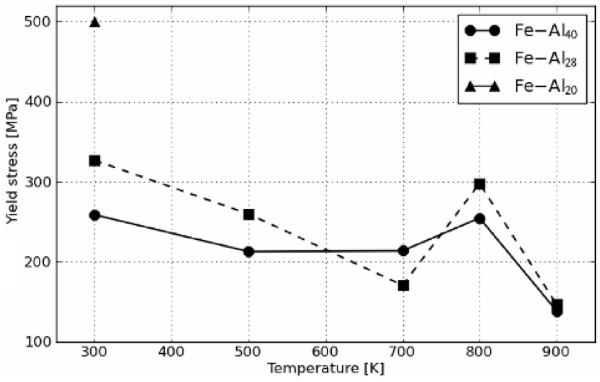

Fig. 4. Dependence of yield stress (0.2% offset) on deformation temperature for three studied alloys.

Fe–Al_{28}, that was not so heavily affected, are presented (Fig. 5).

Slip bands at the temperatures below the YSA peak show common features (Fig. 5a–c): huge primary slip bands correspond to $[1\,\bar{1}\,\bar{1}](1\,0\,1)$ slip system. Weaker secondary slip bands/lines correspond to $[1\,\bar{1}\,\bar{1}](1\,1\,0)$ slip system and are located mainly between the primary slip

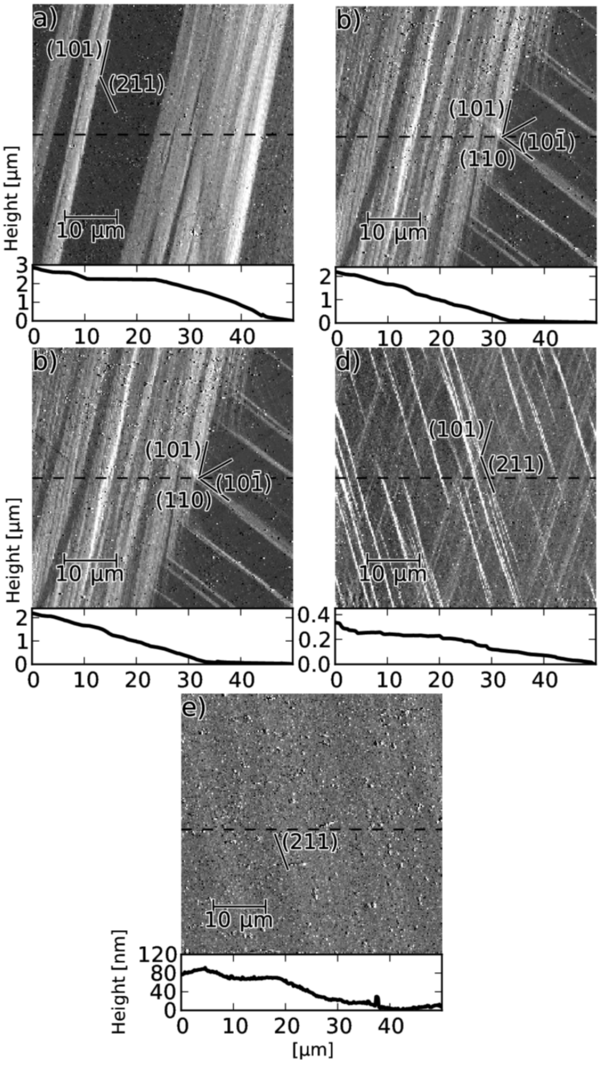

Fig. 5. Surface of Fe–Al_{28} deformed to about 3% plastic strain at different temperatures. (a)–(e) correspond to room temperature, 500, 700, 800 and 900 K respectively. Deformation axis is horizontal, AFM error signal, topography profile across the middle of the image (dashed line) is shown below the images.

bands. Secondary slip lines at room temperature correspond to $[1\,\bar{1}\,\bar{1}](2\,1\,1)$ slip system. Few very weak tertiary lines corresponding to $[1\,1\,1](1\,0\,\bar{1})$ slip system were also observed.

With increasing temperature deformation gets more dispersed. Initially massive and separated slip bands become finer and more homogeneously distributed (Fig. 5a–c).

Slip character changes substantially at peak temperature (Fig. 5d): thin slip lines of two directions are observed. They correspond to the $[1\,\bar{1}\,\bar{1}](1\,0\,1)$ and $[1\,\bar{1}\,\bar{1}](2\,1\,1)$ slip systems. Also the faint structure visible at 900 K (Fig. 5e) seems to correspond to the later slip system.

4. Discussion

As for the wavy slip in *bcc* alloy, any cross-slipped straight crystallographic segments that would form the wavy dislocation trace as suggested by pencil glide model [10] could not be resolved. The resolution of 30×30 μm^2 images is about 60 nm per pixel. Surely, all the magnification and resolution offered by AFM was not utilized. Lateral resolution of AFM is limited by the tip radius that is typically about 10 nm (1–3 nm for super sharp tips [11]). However, due to the localization of slip in the slip bands detailed observation of trace left by single dislocation would be difficult.

The behavior observed *in situ* in the Fe–Al_{28} alloy could be understood on the basis of the following scenario: Dislocations in primary slip band pile-up at an obstacle. With increasing stress some of them are released by the cross-slip to the secondary slip plane. As the stress further increases, dislocations in the primary slip plane overcome the obstacle and tip of the slip band continues to advance until it is stopped again.

Long distance cross-slip to $\{2\,1\,1\}$ type plane observed in the Fe–Al_{28} alloy, contrasts with the *in situ* TEM observations of Rösner et al. [12], who only admits cross-slip to short distances at room temperature. This discrepancy could be accounted for by thin foil effects in the TEM or by the extra stresses due to the dislocation pile up at the tip of the primary slip band in present case.

The formation of texture of weak slip lines in Fe–Al_{40} alloy is clearly not decisive deformation mechanism as the most of the strain is contained within slip bands. Nevertheless, it is of interest as the first manifestation of plastic deformation that occurs during micro-strain yielding.

Deformation axis $[1\,2\,3]$ has been chosen in the middle of the orientation triangle to avoid multiple slip. However, in both Fe–Al_{28} as well as Fe–Al_{40} multiple slip systems were observed. The *in situ* observations suggest that slip bands appearing first correspond to the $[1\,\bar{1}\,\bar{1}](1\,0\,1)$ slip system. This is the $\langle 1\,1\,1\rangle\{0\,1\,1\}$ type slip system with maximum Schmid factor of 0.467. Both secondary $[1\,\bar{1}\,\bar{1}](1\,1\,0)$ and tertiary $[1\,1\,1](1\,0\,\bar{1})$ slip systems have the same lower Schmid factor of 0.350. They are observed in the later stages of deformation when the hardening of primary system could have already started. Secondary system $[1\,\bar{1}\,\bar{1}](2\,1\,1)$ observed in Fe–Al_{28} has the Schmid factor of 0.471.

Different Burgers vector of tertiary slip system is well illustrated by black and white slip lines on AFM error signal images (Fig. 5b,c). This corresponds to the difference in the step direction (step up vs. step down) across the slip lines created by dislocations with different Burgers vectors.

Gradual broadening and leveling of slip bands with increasing temperature observed in Fe–Al_{28} (Fig. 5a–c) is in accordance with Brinck et al. [5] and could be attributed to the thermally activated cross-slip. Weak structure visible at highest temperature (Fig. 5e), may actually be very fine homogeneous slip as reported by Engelke and Neuhäuser [4]. However, surface degradation due to the oxidation cannot be ruled out.

5. Summary

AFM observations of deformed surfaces of three Fe–Al compounds were presented. Formation of wavy slip band in *bcc* Fe–Al_{20}, cross-slip of dislocations from primary slip band to secondary slip lines in Fe–Al_{28} and the evolution of fine slip line texture between the slip bands in Fe–Al_{40} were observed *in situ*. Surfaces of Fe–Al_{28} deformed at different temperatures were observed *post mortem*. Changes in the character of slip, in the temperature range of YSA were described. Although, focus was put on a qualitative description of deformed surfaces, AFM data offer plenty of quantitative information that could be further exploited.

Acknowledgments

This work was supported by following grants: GAUK 23510, SVV 2011-263303, MSM 0021620834, and P107/10/0438. J. Veselý gratefully acknowledges the scholarship of the French government.

References

[1] J.T. Guo, O. Jin, W.M. Yin, T.M. Wang, *Scr. Metall. Mater.* **29**, 783 (1993).

[2] D.G. Morris, M.A. Muñoz-Morris, *Intermetallics* **13**, 1269 (2005).

[3] J. Bonneville, C. Coupeau, *Mater. Sci. Eng. A* **483--484**, 87 (2008).

[4] C. Engelke, H. Neuhäuser, *Scr. Metall. Mater.* **33**, 1109 (1995).

[5] A. Brinck, C. Engelke, H. Neuhäuser, *Mater. Sci. Eng. A* **234-236**, 418 (1997).

[6] A. Brinck, C. Engelke, H. Neuhäuser, *Mater. Sci. Eng. A* **258**, 37 (1998).

[7] J.H. Schneibel, L. Martínez, *J. Mater. Res.* **10**, 2159 (1995).

[8] J. Man, M. Petrenec, K. Obrtlík, J. Polák, *Acta Mater.* **52**, 5551 (2004).

[9] C. Coupeau, J.C. Girard, J. Grilhé, *J. Vac. Sci. Technol. B* **16**, 1964 (1998).

[10] G.I. Taylor, C.F. Elam, *Proc. R. Soc. Lond. A* **112**, 337 (1926).

[11] D. Klinov, S. Magonov, *Appl. Phys. Lett.* **84**, 2697 (2004).

[12] H. Rösner, G. Molénat, E. Nembach, *Mater. Sci. Eng. A* **216**, 169 (1996).